Check for updates

Research Article

INTERNATIONAL JOURNAL OF ADVANCED ROBOTIC SYSTEMS

International Journal of Advanced Robotic Systems
January-February 2018: 1–17
© The Author(s) 2018
DOI: 10.1177/1729881417752758
journals.sagepub.com/home/arx
SAGE

Study on structural modeling and kinematics analysis of a novel wheel-legged rescue robot

Jianye Niu[1,2], Hongbo Wang[1,2], Hongmin Shi[1,2], Nicolae Pop[3], Dong Li[1,2], Shanshan Li[1,2] and Shaozhen Wu[1,2]

Abstract

This article presents a novel rescue robot with three-degrees of freedom leg mechanism based on the serial–parallel and wheel-legged mechanisms, which consists of two *U*niversal joint-*P*rismatic joint-*S*pherical joint plus one *U*niversal joint and *R*evolute joint serial–parallel mechanism. Firstly, the structure model of the whole mechanism and the leg mechanism is developed, the dimension parameters of leg mechanism are designed, and the degrees of freedom of the whole mechanism and the leg mechanism is analyzed. Secondly, the forward and backward position solutions of the swing leg and the standing leg are solved, and the work space is obtained. Thirdly, the kinematics is investigated by the influence coefficient method, including the Jacobi matrix and linear velocity and angular velocity of each rod's centroid of the leg mechanism. Finally, the simulation and experiment are carried out, and the feasibility of this wheel-legged rescue robot and the correctness of the above research are verified.

Keywords

Rescue robot, serial–parallel mechanism, wheel-legged mechanism, kinematics analysis, experiment research

Date received: 10 August 2017; accepted: 4 December 2017

Topic: Special Issue—Mobile Robots
Topic Editor: Manuel Angel Armada Rodriguez
Associate Editor: Michal Kelemen

Introduction

With the improvement of robots' performance, the mobile robot can play a key role in our lives in the near future. The mobile robot has been used in wide range of application, they can not only be used in service industry, such as manufacture industry, agriculture, national defense, and healthcare field but also can be widely used in some extremely dangerous situations such as mine clearance, search-and-rescue in the earthquake area, radiation area, and other special field. Therefore, technology of mobile robots has drawn the worldwide attention.[1–3]

Two types of mobile robot are studied at present, which are wheeled mobile robot and legged mobile robot. For the two types, they have both advantages and disadvantages. The advantages of the wheeled robot are fast moving speed, high energy utilization, simple control method, and low cost. But the disadvantages are poor obstacle avoidance ability and poor complex terrain adaptation ability. However, in these respects, legged robot and wheel robot are the opposite.[4] To develop the advantages and avoid the

[1] Parallel Robot and Mechatronic System Laboratory of Hebei Province, Yanshan University, Qinhuangdao, China
[2] Key Laboratory of Advanced Forging & Stamping Technology and Science of Ministry of Education, Yanshan University, Qinhuangdao, China
[3] Institute of Solid Mechanics, Romanian Academy, Bucharest, Romania

Corresponding author:
Hongbo Wang, Parallel Robot and Mechatronic System Laboratory of Hebei Province, Yanshan University, Qinhuangdao 066004, China.
Email: hongbo_w@ysu.edu.cn

Creative Commons CC BY: This article is distributed under the terms of the Creative Commons Attribution 4.0 License (http://www.creativecommons.org/licenses/by/4.0/) which permits any use, reproduction and distribution of the work without further permission provided the original work is attributed as specified on the SAGE and Open Access pages (https://us.sagepub.com/en-us/nam/open-access-at-sage).

disadvantages, the two types of mobile robot are combined into wheel-legged mobile robot, and the robot adopts wheeled model in flat terrain and legged model in rugged terrain. The wheel-legged robot can improve the moving speed and adaptability in some complex land conditions. So the wheel-legged robot has become a new research and development direction of the mobile robot. The wheel-legged mobile robot has been widely studied at home and abroad.

The Mars rover sojourner[5] and ATHLETE[6] were developed by the Jet Propulsion Laboratory, USA. The skating robot Roller-Walker was developed by the Tokyo Institute of Technology, Japan.[7,8] The combined wheeled and legged robot ALDURO was developed by Gerhard Mercator University, Duisburg, Germany.[9] The wheel-legged robot Hylos was developed by Pierre and Marie Curie University, France.[10] The Octopus robot was developed by the Swiss Federal Institute of Technology Zürich, Switzerland.[11] The wheel-legged robot LegVan was developed by the Wrocław University of Technology, Poland.[12] A hybrid wheeled-leg robot PAW was developed by McGill University, Canada.[13]

In China, many universities and research institutes devoted to the study of the wheel-legged robot. The Harbin Institute of Technology, Beijing, developed the wheel-legged robot, HIT-HYBTOR[14] and HITAN-I.[15]

The University of Aeronautics and Astronautics proposed the robot NOROS,[16] the University of Science and Technology of China designed a leg-wheel robot HyTRo-I,[17] National Taiwan University developed Quattroped, a leg-wheel transformable robot,[18] and Chongqing University proposed the robot Rolling-Wolf.[19]

For the legged walking robot, the quadruped with superior walking and load capacity are the main bionic objects, such as horses, donkeys, cattle, camels, and so on. Shigeo Hirose, the scholar from the Tokyo Institute of Technology, thinks that the quadruped walking robot is the best form of the legged walking robot in the robot's stability, the difficulty of control, and the manufacturing cost.[20]

There are two types of robot in structure, the serial mechanism and the parallel mechanism. Because of the closed-loop mechanism, parallel mechanism, compared with the serial mechanism, has the advantages of strong bearing capacity and high precision, but also has the disadvantages of small work space and end-effector inflexible. If the serial mechanism and the parallel mechanism are combined, it will further expand the application field of robot. The mechanism has the combining advantages of series mechanism and parallel mechanism. It overcomes small work space and can achieve high precision and strong bearing capacity.[21]

When a new mechanical structure is put forward, the degree of freedom (DOF) should be studied first, such as the number of independent movements, and the characteristic of motion.[22] The work space is the important performance index to evaluate the robot. It is meaningful to study the relation between the structure parameter and the work space, and the bigger work space can be obtained by the optimal design.[23]

The kinematics analysis of the robot play a critical role in the parameters design and performance analysis of the robot.[24] The Jacobi matrix of the robot reflects the nature of the kinematics, and Jacobi matrix can easily express agency velocity analysis, error analysis, and force analysis. It can do in-depth analysis in the robot's performance, such as special shape of mechanism, drive space and work space of robot, the flexibility of the robot arm, isotropy, and operating availability.[25] There are many methods of kinematics analysis, such as derivative method, influence coefficient method, vector method, and loop equation method. The derivative method is the derivation of the position motion expression. The more the member is, the more complicated the calculation is, so it is suitable for the case of few rods. Especially, the expression of kinematics relation is clear and simple by the influence coefficient method. In this article, the kinematics problems will be solved by the derivative method and the influence coefficient method.[26]

This article is organized as follows. In the second section, the structure model and design parameters are described, and the DOF of the single leg and the whole mechanism is calculated. In the third section, the forward and backward position solutions of the swing leg and the standing leg are solved, and work space is obtained by the spherical coordinate search method. In the fourth section, the kinematics of the mechanism is solved by the influence coefficient method. In the fifth section, the kinematics simulation is carried out by the ADAMS (Adams 2013) and MATLAB (MATLAB R2014a) software. In the sixth section, the motion experiment of the single leg mechanism and the trajectory tracking experiment are conducted.

Structure model of the wheel-legged rescue robot

Model introduction

According to biological theory, walking of human and animals is achieved by the contraction and relaxation of the skeletal muscles, which leads to the movement of bones. Most skeletal muscles are attached to the bones by means of the tendons, as shown in Figure 1. The arrangement of the skeletal muscles is very similar to the parallel mechanism, while the series mechanism is basically modeled on the arrangement of the skeleton. Therefore, the serial–parallel mechanism is closer to the bionic in the way of layout.

Based on the above research on the distribution of muscle structure, a single leg mechanism is presented, which is a two Universal-Prismatic-Spherical plus one Universal and Revolute (meaning (2-UPS+U) &R) serial–parallel mechanism based on the serial–parallel and wheel-legged mechanisms with 3-DOF, as shown in Figure 2. In the structure, the two electric pushing rods simulate the muscle distribution of the animal's leg to drive the upper leg swing in two directions (2-UPS+U). The robot's upper leg and lower leg are connected by a revolute joint (R) in series,

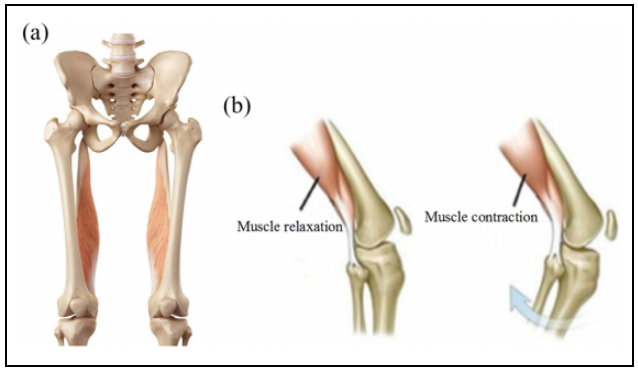


Figure 1. Principle of animal walking. (a) Leg structure of human and (b) schematic diagram of skeletal muscle.

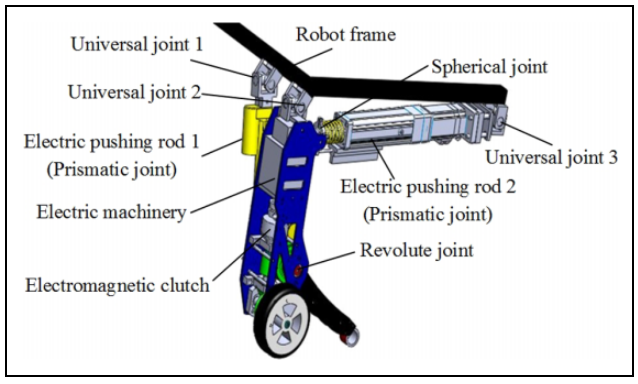


Figure 2. Single leg model of the wheel-legged rescue robot.

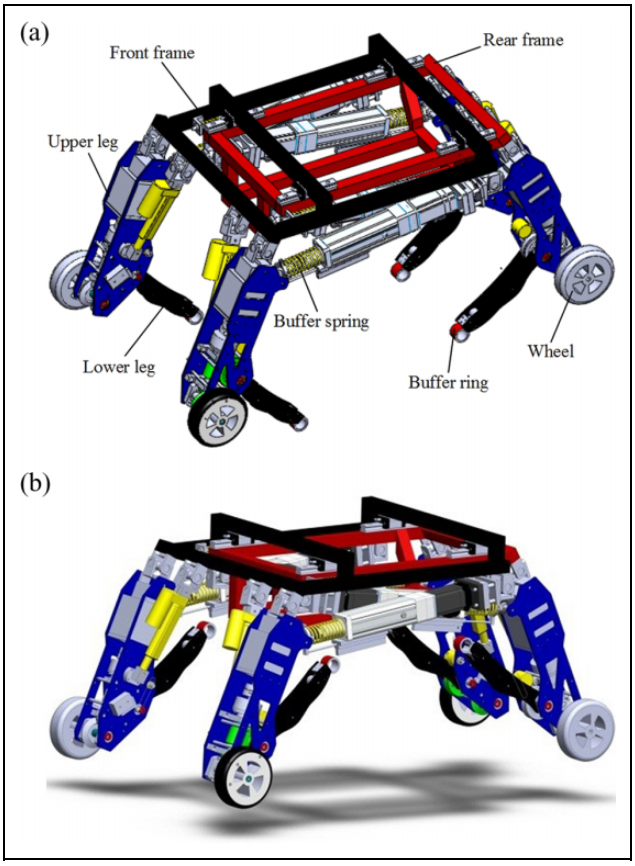


Figure 3. Structure model of the wheel-legged rescue robot. (a) Legged mode and (b) wheeled mode.

which simulate the distribution of the skeleton. The wheel is mounted on the outside of the knee joint, which does not affect the flexibility of the lower leg's movement. This is better than being installed on the foot-end.

Figure 3 shows the structure model of the wheel-legged rescue robot. The robot is composed of the framework and four legs of the same structures. The robot has two moving modes, legged mode and wheeled mode. In the legged mode, the lower legs contact with the ground which is equivalent to a quadruped walking robot. Each leg is a (2-UPS+U) &R serial–parallel mechanism which consists of an upper leg and a lower leg, and the leg mechanism has 3-DOF. In the wheeled mode, the lower legs retract and the wheels contact with the ground, which is equivalent to a four-wheel mobile robot and the speed is fast. At this moment, each leg is a parallel structure and has 2-DOF, so that the robot has the advantages of large load and good rigidity, and its flexibility and carrying capacity are greatly improved.

Parameters setting and coordinate system description

By reading the literature materials at home and abroad, the status quo of the walking robots were studied. According to the analysis of the requirements of the robot's speed and load for rescue mission, the dimension parameters of the whole robot are given, as shown in Table 1. The desired

Table 1. Dimension parameters of the whole robot.

Parameter names	Parameter values
Length of the robot	720 mm
Width of the robot	600 mm
Maximum height	520 mm
Maximum speed of the legged mode	0.4 m s^{-1}
Maximum speed of the wheeled mode	2.2 m s^{-1}
Maximum load	80 kg
Maximum obstacle height	200 mm

maximum load of the robot studied is 80 kg, the speed in the legged mode and the wheeled mode is 1.5 and 8 km h^{-1}, respectively, and the maximum obstacle height is 200 mm.

According to the design target of the robot, the DOF, workspace, and kinematics were studied, and each dimension was optimized. Finally, the range of motion and maximum speed of each input rod and joint is given, as shown in Table 2. The design parameters of each rod of the leg mechanism are brought forward, as shown in Table 3. The schematic diagram of the single leg mechanism is shown in Figure 4.

Based on all the members are rigid bodies, the coordinate system of the swing leg mechanism should be built first, and assuming that the leg coordinate system is the forward leg of the whole machine, as shown in Figure 4.

Table 2. The range of input rod and joint motion and maximum speed of the leg mechanism.

Parameter names	Parameter values
Length of the input rod l_{01}	289–350 mm
Length of the input rod l_{02}	596–740 mm
Rotation angle of the knee joint	-90° to 0°
Speed of the input rod l_{01}	15 mm s^{-1}
Speed of the input rod l_{02}	200 mm s^{-1}
Angular velocity of the knee joint	2 rad s^{-1}

Table 3. Dimension parameters of the leg mechanism (mm).

Parameter names	Parameter values
Length of the upper platform side a_1	130
Length of the upper platform side a_2	650
Length of the upper leg l_1	350
Length of the lower leg l_2	290
Length of the connecting rod between the upper leg and the input rods $b = c$	60
Length of Z_{KB}	70
Length of Z_{KC}	270

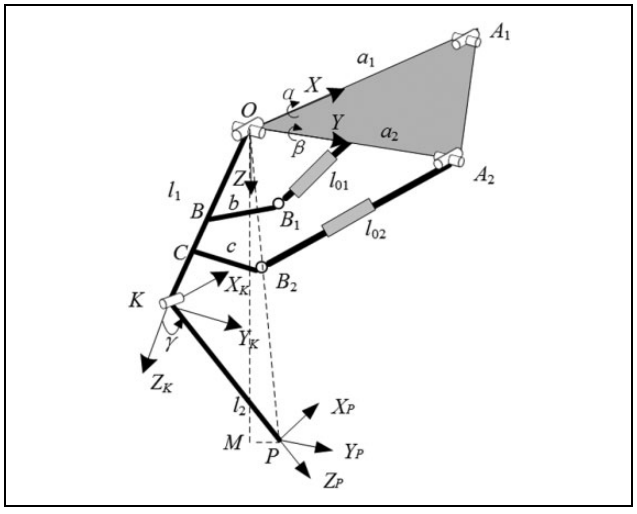


Figure 4. The coordinate systems of a leg.

The fixed coordinate system *O*-*XYZ* is set up at the point *O* on the upper platform, in which the *X*-axis and the *Y*-axis are parallel to the two sides of the upper platform, OA_1 and OA_2, and the *Z*-axis is perpendicular to the upper platform by the right-hand rule. The dynamic coordinate system K-$X_KY_KZ_K$ of the upper leg is established at the knee joint *K*, in which the X_K-axis coincides with the axis of the rotation joint, the Z_K-axis is downward along the *OK* direction of the upper leg rod, and the direction of Y_K-axis is determined according to the right-hand rule. The dynamic coordinate system P-$X_PY_PZ_P$ of the lower leg is established at the point *P*, in which the X_P-axis is parallel to the X_K-axis, the Z_P-axis is downward along the *KP* direction of the upper leg, and the direction of Y_P-axis is determined according to the right-hand rule.

DOF analysis

The DOF of single leg can be calculated using the Kutzbach–Grübler criterion

$$M = d(n - g - 1) + \sum_{i=1}^{g} f_i + v - \zeta = 6 \times (7 - 8 - 1) + 15 + 0 - 0 = 3 \quad (1)$$

where *M* denotes the number of DOF, *n* denotes the number of links, *g* denotes the number of joints, f_i denotes the DOF corresponding to the *i*th joint, *v* denotes the number of redundancy, and ζ denotes the number of isolated DOF.

The DOF of the wheel-legged rescue robot is divided into the following modes:

1. Mode of standing: The robot with the end of four legs directly contact with the ground. The DOF is

$$M = d(n - g - 1) + \sum_{i=1}^{g} f_i + v - \zeta = 6 \times (26 - 36 - 1) + 72 + 0 + 0 = 6 \quad (2)$$

2. Model of static walking of quadruped: When the robot is in the walking, it can be ensured that only one leg as a swing leg stepped forward and the remaining three legs as a foot standing leg support body. The DOF is

$$M = d(n - g - 1) + \sum_{i=1}^{g} f_i + v - \zeta = 6 \times (20 - 27 - 1) + 54 + 0 + 0 = 6 \quad (3)$$

3. Model of dynamic walking of quadruped: When the robot is in the walking, it can be ensured that any two legs as a swing leg stepped forward and the other two legs as a foot standing leg support body. The DOF is

$$M = d(n - g - 1) + \sum_{i=1}^{g} f_i + v - \zeta = 6 \times (14 - 18 - 1) + 36 + 0 + 0 = 6 \quad (4)$$

Through the solution of above three modes of freedom, it can be learned whether the robot is in standing or walking mode, no matter how many legs support the body, the DOF is 6. From the above analysis, the leg mechanism and mechanism of the robot's DOFs can meet the requirements of walking robot.

The above analysis shows that the DOF of leg mechanism is 3. Based on the screw theory, the constraint of leg mechanism and basic movement is analyzed, and the kinematics of leg mechanism is solved.

Under the coordinate system on the fixed platform, the helix of each motion pair of leg mechanism can be shown as: the hook joint between upper leg mechanism and fixed platform is equivalent to two revolute pairs, equates to two

helixes, $\$_1$ and $\$_2$; the revolute pair between the upper leg and the lower leg has a helix $\$_3$; therefore, the kinematics screw system of leg mechanism can be shown as follows

$$\begin{aligned} \$_1 &= (1\ \ 0\ \ 0\,;0\ \ 0\ \ 0) \\ \$_2 &= (0\ \ 1\ \ 0\,;0\ \ 0\ \ 0) \\ \$_3 &= (1\ \ 0\ \ 0\,;0\ \ y\ \ 0) \end{aligned} \tag{5}$$

To solve the reciprocal screw of the kinematics screw system of wheel-legged rescue robot, we can get the restrict screw system of leg mechanism

$$\begin{aligned} \$_1^r &= (1\ \ 0\ \ 0\,;0\ \ 0\ \ 0) \\ \$_2^r &= (0\ \ 1\ \ 0\,;0\ \ 0\ \ 0) \\ \$_3^r &= (0\ \ 0\ \ 0\,;0\ \ 0\ \ 1) \end{aligned} \tag{6}$$

It can be seen from equation (6), the leg mechanism has three restrict screws, $\$_1^r$, $\$_2^r$, and $\$_3^r$, they constraint the motion along the X-axis, the Y-axis, and the rotation of the Z-axis of the leg mechanism. So, the leg mechanism can achieve the rotation of the X-axis and Y-axis, and the motion along the Z-axis.

Position analysis

Position analysis of the swing leg

At first, to solve the position analysis of the swing leg, the relationship between the lengths of two branched chain l_{01} and l_{02}, joint angle γ, and the position vector of leg endpoint P. The position vector $\boldsymbol{P}$ and rotation angle are defined in fixed coordinate system $\{O\}$.

From above, we can know that the dynamic coordinate system K-$X_KY_KZ_K$ can be achieved by the position of the fixed coordinate system O-XYZ through two turns. At first, moving round the X-axis with a rotate angle α, and moving round the Y-axis with a rotate angle β; otherwise, the dynamic coordinate system P-$X_PY_PZ_P$ can be gotten by the dynamic coordinate system K-$X_KY_KZ_K$, which move round the Y_K-axis with a rotate angle γ. So, the transformation matrix can be obtained as follows

$$\begin{aligned} {}^O_K\boldsymbol{R} &= \mathrm{Rot}(X,\alpha)\,\mathrm{Rot}(Y,\beta) \\ &= \begin{bmatrix} 1 & 0 & 0 \\ 0 & \mathrm{c}\alpha & -\mathrm{s}\alpha \\ 0 & \mathrm{s}\alpha & \mathrm{c}\alpha \end{bmatrix} \begin{bmatrix} \mathrm{c}\beta & 0 & \mathrm{s}\beta \\ 0 & 1 & 0 \\ -\mathrm{s}\beta & 0 & \mathrm{c}\beta \end{bmatrix} \\ &= \begin{bmatrix} \mathrm{c}\beta & 0 & \mathrm{s}\beta \\ \mathrm{s}\alpha\,\mathrm{s}\beta & \mathrm{c}\alpha & -\mathrm{s}\alpha\,\mathrm{c}\beta \\ -\mathrm{c}\alpha\,\mathrm{s}\beta & \mathrm{s}\alpha & \mathrm{c}\alpha\,\mathrm{c}\beta \end{bmatrix} \end{aligned} \tag{7}$$

$$ {}^K_P\boldsymbol{R}^P = \mathrm{Rot}(X_K,\gamma) = \begin{bmatrix} 1 & 0 & 0 \\ 0 & \mathrm{c}\gamma & -\mathrm{s}\gamma \\ 0 & \mathrm{s}\gamma & \mathrm{c}\gamma \end{bmatrix} \tag{8}$$

where $\mathrm{s}\alpha = \sin\alpha$, $\mathrm{c}\alpha = \cos\alpha$, $\mathrm{s}\beta = \sin\beta$, $\mathrm{c}\beta = \cos\beta$, $\mathrm{s}\gamma = \sin\gamma$, and $\mathrm{c}\gamma = \cos\gamma$.

In the fixed coordinate system O-XYZ, the initial coordinate of the point K is $[0\ 0\ l_1]^{\mathrm{T}}$. After the rotation, the coordinate of the point K can be obtained as follows

$$ {}^O_K\boldsymbol{K} = {}^O_K\boldsymbol{R}\cdot\boldsymbol{K} = [\,l_1\,\mathrm{s}\beta \quad -l_1\,\mathrm{s}\alpha\,\mathrm{c}\beta \quad l_1\,\mathrm{c}\alpha\,\mathrm{c}\beta\,]^T \tag{9}$$

Therefore, the rotation coordinate matrix that the dynamic coordinate system K-$X_KY_KZ_K$ relatives to the fixed coordinate system O-XYZ is

$$ {}^O_K\boldsymbol{T} = \begin{bmatrix} \mathrm{c}\beta & 0 & \mathrm{s}\beta & l_1\,\mathrm{s}\beta \\ \mathrm{s}\alpha\,\mathrm{s}\beta & \mathrm{c}\alpha & -\mathrm{s}\alpha\,\mathrm{c}\beta & -l_1\,\mathrm{s}\alpha\,\mathrm{c}\beta \\ -\mathrm{c}\alpha\,\mathrm{s}\beta & \mathrm{s}\alpha & \mathrm{c}\alpha\,\mathrm{c}\beta & l_1\,\mathrm{c}\alpha\,\mathrm{c}\beta \\ 0 & 0 & 0 & 1 \end{bmatrix} \tag{10}$$

In the dynamic coordinate system K-$X_KY_KZ_K$, the initial coordinate of the point P is $[0\ 0\ l_2]^{\mathrm{T}}$. After the rotation, the coordinate of the point P can be obtained as follows

$$ {}^K_P\boldsymbol{P} = {}^K_P\boldsymbol{R}\cdot\boldsymbol{P} = [\,0 \quad -l_2\,\mathrm{s}\gamma \quad l_2\,\mathrm{c}\gamma\,]^T \tag{11}$$

Therefore, the rotation coordinate matrix that the dynamic coordinate system P-$X_PY_PZ_P$ relatives to the dynamic coordinate system K-$X_KY_KZ_K$ is

$$ {}^K_P\boldsymbol{T} = \begin{bmatrix} 1 & 0 & 0 & 0 \\ 0 & \mathrm{c}\gamma & -\mathrm{s}\gamma & -l_2\,\mathrm{s}\gamma \\ 0 & \mathrm{s}\gamma & \mathrm{c}\gamma & l_2\,\mathrm{c}\gamma \\ 0 & 0 & 0 & 1 \end{bmatrix} \tag{12}$$

The rotation coordinate matrix that the moving coordinate system P-$X_PY_PZ_P$ relatives to the fixed coordinate system O-XYZ is

$$ {}^O_P\boldsymbol{T} = {}^O_K\boldsymbol{T}\,{}^K_P\boldsymbol{T} \tag{13}$$

By the transformation matrixes, in the fixed coordinate system O-XYZ, the coordinate of the endpoint P can be obtained as follows

$$\begin{aligned} p_x &= l_2\,\mathrm{s}\beta\,\mathrm{c}\gamma + l_1\,\mathrm{s}\beta \\ p_y &= -l_2\,\mathrm{c}\alpha\,\mathrm{s}\gamma - l_2\,\mathrm{s}\alpha\,\mathrm{c}\beta\,\mathrm{c}\gamma - l_1\,\mathrm{s}\alpha\,\mathrm{c}\beta \\ p_z &= -l_2\,\mathrm{s}\alpha\,\mathrm{s}\gamma + l_2\,\mathrm{c}\alpha\,\mathrm{c}\beta\,\mathrm{c}\gamma + l_1\,\mathrm{c}\alpha\,\mathrm{c}\beta \end{aligned} \tag{14}$$

According to the coordinate system established in Figure 4, the coordinates of the points on the upper leg rod in each coordinate system can be obtained as follows

$$\begin{aligned} {}^OA_1 &= \begin{bmatrix} a_1 \\ 0 \\ 0 \end{bmatrix} \quad {}^OA_2 = \begin{bmatrix} 0 \\ a_2 \\ 0 \end{bmatrix} \quad {}^KB_1 = \begin{bmatrix} b \\ 0 \\ -Z_{KB} \end{bmatrix} \\ {}^KB_2 &= \begin{bmatrix} 0 \\ c \\ -Z_{KC} \end{bmatrix} \end{aligned} \tag{15}$$

According to the coordinate of each point and the rotation transformation matrixes of each coordinate system, the length of the input rod l_{01} and l_{02} can be obtained as follows

$$l_{0i} = {}^{O}_{K}\boldsymbol{R}^{K} B_i + {}^{O}\boldsymbol{P}_K - {}^{O}A_i \ (i = 1, 2) \tag{16}$$

So, the length of two input branch can be shown as follows

$$l_{01} = \sqrt{\begin{aligned}&(b_1 \mathrm{c}\beta - Z_{KB}\mathrm{s}\beta + l_1 \mathrm{s}\beta - a_1)^2 \\ &+ (Z_{KB}\mathrm{c}\beta\mathrm{s}\alpha - l_1\mathrm{c}\beta\mathrm{s}\alpha + b_1\mathrm{s}\alpha\mathrm{s}\beta)^2 \\ &+ (l_1\mathrm{c}\alpha\mathrm{c}\beta - Z_{KB}\mathrm{c}\alpha\mathrm{c}\beta - b_1\mathrm{c}\alpha\mathrm{s}\beta)^2\end{aligned}}$$

$$l_{02} = \sqrt{\begin{aligned}&(l_1\mathrm{s}\beta - Z_{KC}\mathrm{s}\beta)^2 \\ &+ (b_2\mathrm{c}\alpha + Z_{KC}\mathrm{c}\beta\mathrm{s}\alpha - l_1\mathrm{c}\beta\mathrm{s}\alpha - a_2)^2 \\ &+ (b_2\mathrm{s}\alpha + l_1\mathrm{c}\alpha\mathrm{c}\beta - Z_{KC}\mathrm{c}\alpha\mathrm{c}\beta)^2\end{aligned}} \tag{17}$$

When the length of l_{01} and l_{02} is the known quantity, according to equation (17), we can get angle α and β. By putting α, β, and γ in equation (14), the position of the endpoint P can be obtained. The above is the forward position analysis of the leg mechanism.

The inverse position problem is that when the position and orientation of the endpoint P are known, to solve the input parameters, the lengths of two branched chain l_{01} and $l_{02,}$ and attitude angle γ.

According to the geometrical relationship of leg mechanism in Figure 4, and using the cosine theorem of triangle, it can be obtained as follows

$$\begin{aligned}\alpha &= \arccos\left(\frac{{l_1}^2 + ({p_x}^2 + {p_y}^2 + {p_z}^2) - {l_2}^2}{2l_1\sqrt{{p_x}^2 + {p_y}^2 + {p_z}^2}}\right) - \arctan\left(\frac{p_y}{p_z}\right) \\ \beta &= \arctan\left(\frac{p_x}{p_z}\right) \\ \gamma &= \pi - \arccos\left(\frac{{l_1}^2 + {l_2}^2 - ({p_x}^2 + {p_y}^2 + {p_z}^2)}{2l_1l_2}\right)\end{aligned} \tag{18}$$

Then, substituting α and β in equation (17), the length of two input branches l_{01} and l_{02} can be obtained.

Position analysis of the standing leg

After analyzing the swing leg, the standing leg is analyzed. The position analysis of the standing leg is to analyze the output pose of the robot's body, which is the relation between the pose of reference point and the input joints. Due to the endpoint of the standing leg is fixed, the fixed coordinate system Q-$X_QY_QZ_Q$ is set up at the endpoint P, as shown in Figure 5. The endpoint of the standing leg is immovable, and the robot's body is pushed by the standing leg. The moving coordinate system O-XYZ is set up at the point O, which is the reference point of the robot's body. The moving coordinate P-$X_PY_PZ_P$ of the lower leg is established at the endpoint P. The moving coordinate system K-$X_KY_KZ_K$ of the upper leg is established at the knee joint between the upper leg and the lower leg.

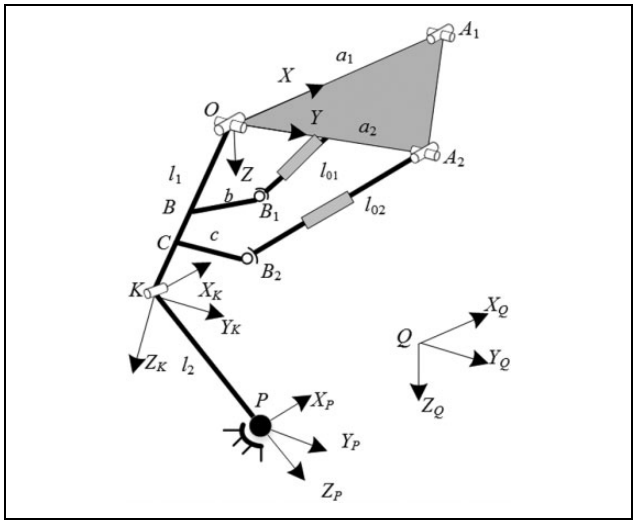


Figure 5. Schematic diagram of standing leg mechanism.

When the leg is used as the standing leg, the relationship between the lower leg and the ground could be equal to a spherical joint, as shown in Figure 5. The angle of the spherical joint turn is φ, ξ, and ς, and the three angles are passive, which are the angles caused by the active joints l_{01}, l_{02}, and γ. In the inverse kinematics of the standing leg, in the series part of the robot, the pose of the robot body is known in the fixed coordinate system. At the initial moment, in the fixed coordinate system Q-$X_QY_QZ_Q$, the coordinate of point O is known and it was marked as ${}^{Q}P_{O1}$, then the standing leg starts to move the body. According to equation (18), α_1, β_1, and γ_1, the initial input values of each input joints, can be obtained. When the standing legs stop moving the body, in the fixed coordinate system Q-$X_QY_QZ_Q$, the coordinate of the reference point O is also known and it was marked as ${}^{Q}P_{O2}$. Then, according to equation (18), α_2, β_2, and γ_2, the input value of each joint at stop time, can be obtained. The total input value of each joint is the input value α_2, β_2, and γ_2, minus the initial input value α_1, β_1, and γ_1.

In the parallel part of the robot, the obtained joint input values α and β are the output value of the parallel part. Therefore, the coordinate transformation matrix of the upper leg coordinate system $\{K\}$ relative to the fixed coordinate system $\{Q\}$ must be solved when the input values l_{01} and l_{02} of the electric pushing rods are required to be solved. According to the following

$${}^{Q}_{K}\boldsymbol{T} = {}^{Q}_{O}\boldsymbol{T} \cdot {}^{O}_{K}\boldsymbol{T} \tag{19}$$

where ${}^{Q}_{O}\boldsymbol{T}$ is known, and ${}^{O}_{K}\boldsymbol{T}$ was obtained in equation (11).

Table 4. The constraints of work space of the leg mechanism.

Constraints	Constrained parameter	Parameter values
Length constraint of the drive rod	Input rod l_{01} and l_{02}	289 mm $\leq l_{01} \leq$ 350 mm 596 mm $\leq l_{02} \leq$ 740 mm
Angle constraint of the universal joints	Universal joint at point O	$-5^\circ \leq \alpha \leq 55^\circ$ $-25^\circ \leq \beta \leq 25^\circ$
	Universal joint at point A_1	$-5^\circ \leq \alpha \leq 55^\circ$ $-25^\circ \leq \beta \leq 25^\circ$
	Universal joint at point A_2	$-5^\circ \leq \alpha \leq 55^\circ$ $-25^\circ \leq \beta \leq 25^\circ$
Angle constraint of the spherical joints	Spherical joints at points B_1 and B_2	$0^\circ \leq \eta \leq 40^\circ$
Angle constraint of the revolute joint	Revolute joint at point K	$0^\circ \leq \gamma \leq 90^\circ$

The input value of the electric pushing rods in the parallel part of the robot is as follows

$$l_{0i} = ({}^{O}_{K}\boldsymbol{R} \cdot {}^{K}B_i + {}^{O}\boldsymbol{P}_K) - ({}^{O}_{O}\boldsymbol{R} \cdot {}^{O}A_i + {}^{O}\boldsymbol{P}_O) \quad (i = 1, 2) \tag{20}$$

Work space analysis

While planning robot gait, the foot trajectory must be guaranteed in the reachable mechanism work space. And the work space determines dexterity and the maneuverability of the mechanism. Thus, the work space is one of the most important aspects and it is very necessary to analyze the shape and the volume of the work space.

According to the above position analysis, the constraints of the work space of the leg mechanism are necessary to be determined.

1. Constraints of the length of the input rods

   The length of the input rods l_{0i} $(i = 1, 2)$ needs to meet the following

$$l_{\min} \leq l_{0i} \leq l_{\max} \tag{21}$$

2. Constraints of the corner of hook joint and spherical joint

   The corner of hook joint δ_i needs to meet the following

$$\delta_i \leq \delta_{i\max} \tag{22}$$

   The corner of spherical joint η_i is

$$\eta_i = \arccos\left(\frac{\boldsymbol{q}_i \cdot \boldsymbol{l}_{0i}}{||q_i|| \times ||l_{0i}||}\right) \tag{23}$$

   The corner of spherical hinge η_i needs to meet the following

$$0 \leq \eta_i \leq \eta_{i\max} \tag{24}$$

3. Constraints of each rod

   In order to avoid interference, it needs to meet the following

$$d_{ij} \geq d \tag{25}$$

The constraints and design parameters for the leg mechanism of the rescue robot are shown in Table 4.

In order to obtain the work space of the leg mechanism of the robot, the spherical coordinate search method is used. According to the designed parameters of the leg mechanism, the work space of the leg mechanism is obtained with MATLAB software, as shown in Figure 6.

The work space of the leg mechanism is generally an arc shape, the outer surface is composed of a circular arc, and the inner surface is composed of two concave cambered surfaces. The range of the leg mechanism that can move in the front and back directions is about -300 mm $\leq y \leq$ 300 mm, the range of the leg mechanism that can move in the left and right directions is about -150 mm $\leq x \leq 200$ mm, and the range of the leg mechanism that can lift in the upper and lower directions is -650 mm $\leq z \leq -350$ mm. The work space is larger, and its internal continuity is better. So the work space can meet motion demand of the wheel-legged rescue robot's legs.

Kinematics analysis

Jacobian matrix

The Jacobian matrix of velocity is the matrix that solves the relation between the input velocity and the output velocity.[27] The input velocity of the robot is divided into two parts, the upper leg and the lower leg. The input velocity of the upper leg mechanism is the velocity of the input rods $\dot{l}_{01}$ and $\dot{l}_{02}$, the output velocity is the angular velocity of $\dot{\alpha}$ and $\dot{\beta}$ of the universal pair on the upper leg. The input velocity of the lower leg mechanism is the angular velocity of $\dot{\gamma}$ of the revolute pair on the knee joint.

The angular velocity of $\dot{\alpha}$, $\dot{\beta}$, and $\dot{\gamma}$ is the input velocity of the robot, and the angular velocity and the linear velocity of the lower leg are the output velocity. The endpoint P as the reference point of the lower leg, the angular velocity the point P can be expressed as follows

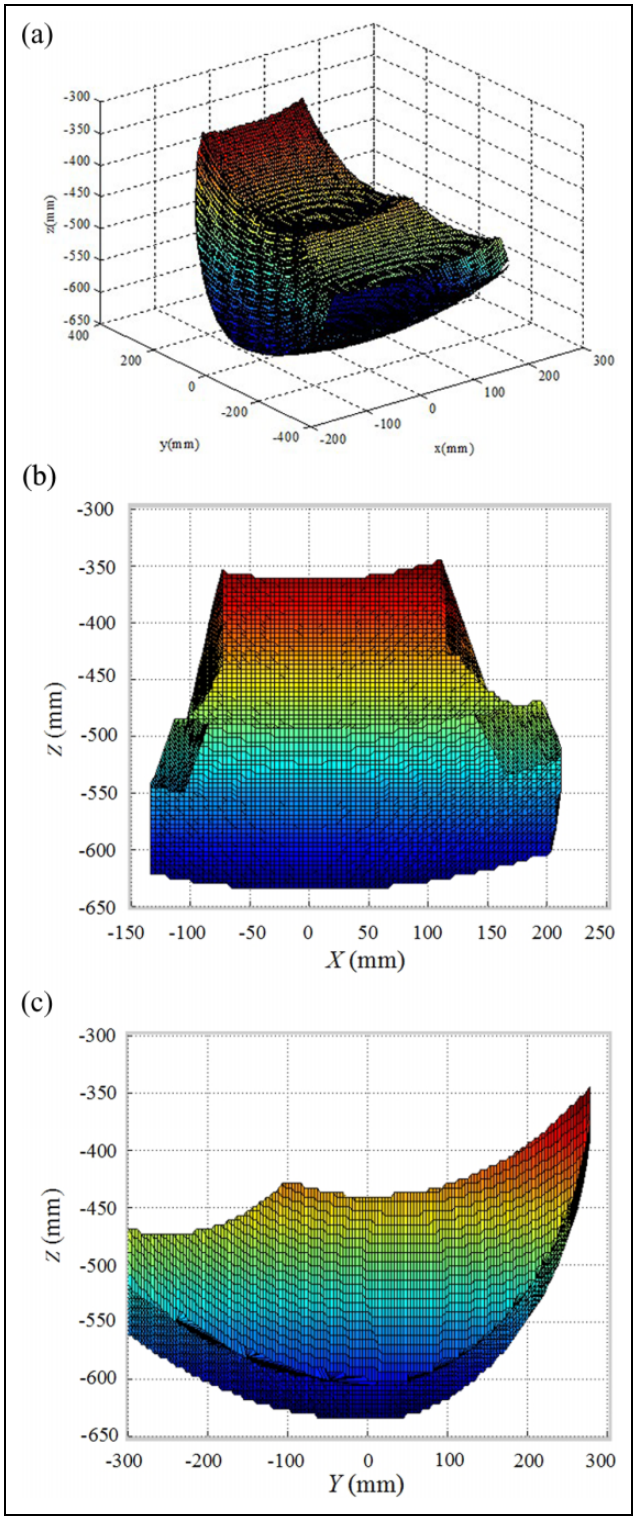


Figure 6. The work space of the leg mechanism. (a) The three-dimensional diagram of the workspace, (b) the projection of the workspace in the *XOZ* plane, and (c) the projection of the workspace in the *YOZ* plane.

$$\begin{aligned} \boldsymbol{w}_p &= \boldsymbol{w}_\alpha + \boldsymbol{w}_\beta + \boldsymbol{w}_K = \dot{\alpha}\cdot\boldsymbol{S}_1 + \dot{\beta}\cdot\boldsymbol{S}_2 + \dot{\gamma}\cdot\boldsymbol{S}_3 \\ &= [\,\boldsymbol{S}_1 \quad \boldsymbol{S}_2 \quad \boldsymbol{S}_3\,] \begin{bmatrix} \dot{\alpha} \\ \dot{\beta} \\ \dot{\gamma} \end{bmatrix} \end{aligned} \tag{26}$$

where $\boldsymbol{S}_1$, $\boldsymbol{S}_2$, and $\boldsymbol{S}_3$ are the unit vectors, $\boldsymbol{S}_1 = [1\ 0\ 0]^{\mathrm{T}}$, $\boldsymbol{S}_2 = [0\ 1\ 0]^{\mathrm{T}}$, and $\boldsymbol{S}_3 = [0\ 0\ 1]^{\mathrm{T}}$.

If the framework serves as a fixed platform, the linear velocity of the endpoint P is caused by the rotation of the three input joints. The linear velocity can be expressed as follows

$$\begin{aligned} \boldsymbol{v}_p &= \dot{\alpha}\cdot\boldsymbol{S}_1 \times {}^{O}\boldsymbol{P} + \dot{\beta}\cdot\boldsymbol{S}_2 \times {}^{O}\boldsymbol{P} + \dot{\gamma}\cdot\boldsymbol{S}_3 \times {}^{O}\boldsymbol{P}_K \\ &= [\,\boldsymbol{S}_1 \times {}^{O}\boldsymbol{P} \quad \boldsymbol{S}_2 \times {}^{O}\boldsymbol{P} \quad \boldsymbol{S}_3 \times {}^{O}\boldsymbol{P}_K\,] \begin{bmatrix} \dot{\alpha} \\ \dot{\beta} \\ \dot{\gamma} \end{bmatrix} \end{aligned} \tag{27}$$

where ${}^{O}P$ is the distance between the endpoint P and the ordinate origin O under the *O-XYZ* coordinate system, and ${}^{O}P_K$ is the coordinates of the endpoint P under the K-$X_KY_KZ_K$ coordinate system to the *O-XYZ* coordinate system.

Simultaneous equations (26) and (27), the velocity of the endpoint P can be obtained as follows

$$\begin{bmatrix} \boldsymbol{w}_p \\ \boldsymbol{v}_P \end{bmatrix} = \begin{bmatrix} \boldsymbol{S}_1 & \boldsymbol{S}_2 & \boldsymbol{S}_3 \\ \boldsymbol{S}_1 \times {}^{O}P & \boldsymbol{S}_2 \times {}^{O}P & \boldsymbol{S}_3 \times {}^{O}P_K \end{bmatrix} \begin{bmatrix} \dot{\alpha} \\ \dot{\beta} \\ \dot{\gamma} \end{bmatrix} \tag{28}$$

It can also be expressed as follows

$$\boldsymbol{V} = \begin{bmatrix} \boldsymbol{w}_p \\ \boldsymbol{v}_p \end{bmatrix} = [\,w_x \quad w_y \quad w_z \quad v_x \quad v_y \quad v_z\,]^{\mathrm{T}} \tag{29}$$

Then, substitute each vector coordinate value into equation (28) and expressed in the form of equation (29), can be obtained as follows

$$\boldsymbol{V} = \begin{bmatrix} w_x \\ w_y \\ w_z \\ v_x \\ v_y \\ v_z \end{bmatrix} = \begin{bmatrix} 1 & 0 & 0 \\ 0 & 1 & 0 \\ 0 & 0 & 0 \\ 0 & p_z & 0 \\ -p_z & 0 & -p_z + l_1\,\mathrm{c}\alpha\,\mathrm{c}\beta \\ p_y & -p_x & p_y + l_1\,\mathrm{s}\alpha\,\mathrm{c}\beta \end{bmatrix} \begin{bmatrix} \dot{\alpha} \\ \dot{\beta} \\ \dot{\gamma} \end{bmatrix} \tag{30}$$

Because the DOF of the leg mechanism is 3, with two rotation DOF and one movement DOF, the output velocity of the leg mechanism can be expressed as follows

$$\boldsymbol{V} = \begin{bmatrix} w_x \\ w_y \\ 0 \\ 0 \\ v_y \\ 0 \end{bmatrix} = \begin{bmatrix} 1 & 0 & 0 \\ 0 & 1 & 0 \\ 0 & 0 & 0 \\ 0 & p_z & 0 \\ -p_z & 0 & -p_z + l_1 \mathrm{c}\alpha \mathrm{c}\beta \\ p_y & -p_x & p_y + l_1 \mathrm{s}\alpha \mathrm{c}\beta \end{bmatrix} \begin{bmatrix} \dot{\alpha} \\ \dot{\beta} \\ \dot{\gamma} \end{bmatrix} \tag{31}$$

Then taking the first row, the second row, and the fifth row from equation (31), the velocity $\boldsymbol{V}$ can be expressed as follows

$$\boldsymbol{V} = \begin{bmatrix} w_x \\ w_y \\ v_y \end{bmatrix} = \begin{bmatrix} 1 & 0 & 0 \\ 0 & 1 & 0 \\ -p_z & 0 & -p_z + l_1 \mathrm{c}\alpha \mathrm{c}\beta \end{bmatrix} \begin{bmatrix} \dot{\alpha} \\ \dot{\beta} \\ \dot{\gamma} \end{bmatrix} \tag{32}$$

The inverse matrix of equation (32) can be obtained as follows

$$\begin{bmatrix} \dot{\alpha} \\ \dot{\beta} \\ \dot{\gamma} \end{bmatrix} = \begin{bmatrix} -\dfrac{p_z - l_2 \mathrm{c}\alpha \mathrm{c}\beta}{l_2 \mathrm{c}\alpha \mathrm{c}\beta} & 0 & \dfrac{p_z}{l_2 \mathrm{c}\alpha \mathrm{c}\beta} \\ 0 & 1 & 0 \\ -\dfrac{1}{l_2 \mathrm{c}\alpha \mathrm{c}\beta} & 0 & \dfrac{1}{l_2 \mathrm{c}\alpha \mathrm{c}\beta} \end{bmatrix} \begin{bmatrix} w_x \\ w_y \\ v_y \end{bmatrix} \tag{33}$$

Equation (33) is the relation between the input velocity of each joint and the output velocity of the endpoint P.

In the upper leg part, the velocity of each joint is the output velocity, and the velocity of push rod is the input velocity. By taking the derivative of equation (17), the following can be obtained

$$\begin{bmatrix} \dot{l}_{01} \\ \dot{l}_{02} \end{bmatrix} = \begin{bmatrix} \boldsymbol{J}_{11} & \boldsymbol{J}_{12} \\ \boldsymbol{J}_{21} & \boldsymbol{J}_{22} \end{bmatrix} \begin{bmatrix} \dot{\alpha} \\ \dot{\beta} \end{bmatrix} = \boldsymbol{J} \begin{bmatrix} \dot{\alpha} \\ \dot{\beta} \end{bmatrix} \tag{34}$$

where $\boldsymbol{J}_{11} = 0$

$$\boldsymbol{J}_{12} = \frac{a_1 l_{OB} \mathrm{c}\beta - a_1 l_1 \mathrm{c}\beta + a_1 b_1 \mathrm{s}\beta}{\sqrt{{a_1}^2 - 2a_1 b_1 \mathrm{c}\beta + 2a_1 l_{OB} \mathrm{s}\beta - 2a_1 l_1 \mathrm{s}\beta + {b_1}^2 + {l_{OB}}^2 - 2l_{OB} l_1 + {l_1}^2}}$$

$$\boldsymbol{J}_{21} = \frac{a_2 b_2 \mathrm{s}\alpha - a_2 l_{OC} \mathrm{c}\alpha \mathrm{c}\beta + a_2 l_1 \mathrm{c}\alpha \mathrm{c}\beta}{\sqrt{{a_2}^2 - 2a_2 b_2 \mathrm{c}\alpha - 2a_2 l_{OC} \mathrm{c}\beta \mathrm{s}\alpha + 2a_2 l_1 \mathrm{c}\beta \mathrm{s}\alpha + {b_2}^2 + {l_{OC}}^2 - 2l_{OC} l_1 + {l_1}^2}}$$

$$\boldsymbol{J}_{22} = \frac{a_2 l_{OC} \mathrm{s}\alpha \mathrm{s}\beta - a_2 l_1 \mathrm{s}\alpha \mathrm{s}\beta}{\sqrt{{a_2}^2 - 2a_2 b_2 \mathrm{s}\alpha - 2a_2 l_{OC} \mathrm{c}\beta \mathrm{s}\alpha + 2a_2 l_1 \mathrm{c}\beta \mathrm{s}\alpha + {b_2}^2 + {l_{OC}}^2 - 2l_{OC} l_1 + {l_1}^2}}$$

When adding $\dot{\gamma}$ into equation (34), it can be expressed as follows

$$\begin{bmatrix} \dot{l}_{01} \\ \dot{l}_{02} \\ \dot{\gamma} \end{bmatrix} = \begin{bmatrix} \boldsymbol{J}_{11} & \boldsymbol{J}_{12} & 0 \\ \boldsymbol{J}_{21} & \boldsymbol{J}_{22} & 0 \\ 0 & 0 & 1 \end{bmatrix} \begin{bmatrix} \dot{\alpha} \\ \dot{\beta} \\ \dot{\gamma} \end{bmatrix} \tag{35}$$

Then putting equation (33) into equation (35), the following can be obtained

$$\begin{bmatrix} \dot{l}_{01} \\ \dot{l}_{02} \\ \dot{\gamma} \end{bmatrix} = \begin{bmatrix} \boldsymbol{J}_{11} & \boldsymbol{J}_{12} & 0 \\ \boldsymbol{J}_{21} & \boldsymbol{J}_{22} & 0 \\ 0 & 0 & 1 \end{bmatrix} \begin{bmatrix} -\dfrac{p_z - l_2 \mathrm{c}\alpha \mathrm{c}\beta}{l_2 \mathrm{c}\alpha \mathrm{c}\beta} & 0 & \dfrac{p_z}{l_2 \mathrm{c}\alpha \mathrm{c}\beta} \\ 0 & 1 & 0 \\ -\dfrac{1}{l_2 \mathrm{c}\alpha \mathrm{c}\beta} & 0 & \dfrac{1}{l_2 \mathrm{c}\alpha \mathrm{c}\beta} \end{bmatrix} \begin{bmatrix} w_x \\ w_y \\ v_y \end{bmatrix} = \boldsymbol{G} \begin{bmatrix} w_x \\ w_y \\ v_y \end{bmatrix} \tag{36}$$

where $\boldsymbol{G}$ is the Jacobian matrix of velocity between the input velocity and the output velocity.

Velocity analysis of each rod in the leg mechanism

The velocity analysis of each rod in the leg mechanism is the basis of the kinematics analysis.

Velocity analysis of the upper leg rod l_1. Calculating the linear velocity and angular velocity at the centroid of the rod l_1. The angular velocity of the rod l_1 is the vector superposition of $\dot{\alpha}$ and $\dot{\beta}$. According to equation (34), the angular velocity can be expressed as follows

$$\boldsymbol{w}_{l_1} = \begin{bmatrix} \dot{\alpha} \\ \dot{\beta} \end{bmatrix} = \boldsymbol{J}^{-1} \begin{bmatrix} \dot{l}_{01} \\ \dot{l}_{02} \end{bmatrix} \tag{37}$$

When adding $\dot{\gamma}$ into equation (37), it can be expressed as follows

$$\boldsymbol{w}_{l_1} = \begin{bmatrix} \boldsymbol{J}^{-1} & \boldsymbol{0} \\ \boldsymbol{0} & 0 \end{bmatrix} \begin{bmatrix} \dot{l}_{01} \\ \dot{l}_{02} \\ \dot{\gamma} \end{bmatrix} \tag{38}$$

Then setting $[\boldsymbol{G}_{l_1}^{w}] = \begin{bmatrix} \boldsymbol{J}^{-1} & \boldsymbol{0} \\ \boldsymbol{0} & 0 \end{bmatrix}$ and $\dot{\boldsymbol{q}} = [\dot{l}_{01} \quad \dot{l}_{02} \quad \dot{\gamma}]^{\mathrm{T}}$, equation (37) can be expressed as follows

$$\boldsymbol{w}_{l_1} = [\boldsymbol{G}_{l_1}^{w}]\dot{\boldsymbol{q}} \tag{39}$$

Because of isotropic material and little deformation, the centroid is considered to be in the middle of the rod l_1. Based on the influence coefficient method, the velocity of the centroid can be expressed as follows

$$\begin{aligned} \boldsymbol{v}_{l_1} &= [\boldsymbol{S}_1 \times {}^{O}\boldsymbol{P}_1 \quad \boldsymbol{S}_2 \times {}^{O}\boldsymbol{P}_1 \quad 0] \begin{bmatrix} \dot{\alpha} \\ \dot{\beta} \\ \dot{\gamma} \end{bmatrix} \\ &= [\boldsymbol{S}_1 \times {}^{O}\boldsymbol{P}_1 \quad \boldsymbol{S}_2 \times {}^{O}\boldsymbol{P}_1 \quad 0] \begin{bmatrix} \boldsymbol{J}^{-1} & \boldsymbol{0} \\ \boldsymbol{0} & 0 \end{bmatrix} \begin{bmatrix} \dot{l}_{01} \\ \dot{l}_{02} \\ \dot{\gamma} \end{bmatrix} \end{aligned} \tag{40}$$

where ${}^{O}\boldsymbol{P}_1$ is the distance from the centroid of the rod l_1 to the origin O of the fixed coordinate system under the fixed coordinate system O-XYZ.

Then setting $[\boldsymbol{G}_{l_1}^{v}] = [\boldsymbol{S}_1 \times {}^{O}\boldsymbol{P}_1 \quad \boldsymbol{S}_2 \times {}^{O}\boldsymbol{P}_1 \quad 0] \begin{bmatrix} \boldsymbol{J}^{-1} & \boldsymbol{0} \\ \boldsymbol{0} & 0 \end{bmatrix}$, equation (40) can be expressed as follows

$$\boldsymbol{v}_{l_1} = [\boldsymbol{G}_{l_1}^{v}]\dot{\boldsymbol{q}} \tag{41}$$

Velocity analysis of the lower leg rod l_2. Based on the influence coefficient method, the angular velocity of the centroid of the rod l_2 can be obtained as follows

$$\boldsymbol{w}_{l_2} = [\boldsymbol{S}_1 \quad \boldsymbol{S}_2 \quad \boldsymbol{S}_3] \begin{bmatrix} \dot{\alpha} \\ \dot{\beta} \\ \dot{\gamma} \end{bmatrix} = [\boldsymbol{S}_1 \quad \boldsymbol{S}_2 \quad \boldsymbol{S}_3] \begin{bmatrix} \boldsymbol{J}^{-1} & \boldsymbol{0} \\ \boldsymbol{0} & 1 \end{bmatrix} \begin{bmatrix} \dot{l}_{01} \\ \dot{l}_{02} \\ \dot{\gamma} \end{bmatrix} \tag{42}$$

Then setting $[\boldsymbol{G}_{l_2}^{w}] = [\boldsymbol{S}_1 \quad \boldsymbol{S}_2 \quad \boldsymbol{S}_3] \begin{bmatrix} \boldsymbol{J}^{-1} & \boldsymbol{0} \\ \boldsymbol{0} & 1 \end{bmatrix}$, equation (42) can be expressed as follows

$$\boldsymbol{w}_{l_2} = [\boldsymbol{G}_{l_2}^{w}]\dot{\boldsymbol{q}} \tag{43}$$

Based on the influence coefficient method, the linear velocity of the centroid of the rod l_2 can be obtained as follows

$$\begin{aligned} \boldsymbol{v}_{l_2} &= [\boldsymbol{S}_1 \times {}^{O}\boldsymbol{P}_2 \quad \boldsymbol{S}_2 \times {}^{O}\boldsymbol{P}_2 \quad \boldsymbol{S}_3 \times {}^{O}_{K}\boldsymbol{P}_2] \begin{bmatrix} \dot{\alpha} \\ \dot{\beta} \\ \dot{\gamma} \end{bmatrix} \\ &= [\boldsymbol{S}_1 \times {}^{O}\boldsymbol{P}_2 \quad \boldsymbol{S}_2 \times {}^{O}\boldsymbol{P}_2 \quad \boldsymbol{S}_3 \times {}^{O}_{K}\boldsymbol{P}_2] \begin{bmatrix} \boldsymbol{J}^{-1} & \boldsymbol{0} \\ \boldsymbol{0} & 1 \end{bmatrix} \begin{bmatrix} \dot{l}_{01} \\ \dot{l}_{02} \\ \dot{\gamma} \end{bmatrix} \end{aligned} \tag{44}$$

where ${}^{O}\boldsymbol{P}_2$ is the centroid coordinate under the fixed coordinate system O-XYZ, ${}^{O}_{K}\boldsymbol{P}_2$ is the distance from the centroid of the rod l_2 to the origin K of the dynamic coordinate system K-$X_KY_KZ_K$ under the fixed coordinate system O-XYZ.

Then setting $[\boldsymbol{G}_{l_2}^{v}] = [\boldsymbol{S}_1 \times {}^{O}\boldsymbol{P}_2 \quad \boldsymbol{S}_2 \times {}^{O}\boldsymbol{P}_2 \quad \boldsymbol{S}_3 \times {}^{O}_{K}\boldsymbol{P}^{K}{}_2] \begin{bmatrix} \boldsymbol{J}^{-1} & \boldsymbol{0} \\ \boldsymbol{0} & 1 \end{bmatrix}$, equation (44) can be expressed as follows

$$\boldsymbol{v}_{l_2} = [\boldsymbol{G}_{l_2}^{v}]\dot{\boldsymbol{q}} \tag{45}$$

Velocity analysis of the electric pushing rod. The electric pushing rod is composed of a pushing rod and an electric cylinder. The length of the pushing rod changes in real time, so the centroid of electric pushing rod is changed. Because the mass of the pushing rod is smaller than the mass of the electric push cylinder, so the position of the centroid is located in the upper part of the pushing rod, which is between the electric push cylinder and the Universal pair. Therefore, the angular velocity and linear velocity of the centroid of the electric pushing rod are determined by the Universal pair fixed on the frame.

According to equations (38) to (41), and based on the influence coefficient method, the angular velocity of point B_i ($i = 1, 2$) can be obtained as follows

$$\boldsymbol{w}_{B_i} = \boldsymbol{w}_{l_1} = \begin{bmatrix} \boldsymbol{J}^{-1} & \boldsymbol{0} \\ \boldsymbol{0} & 0 \end{bmatrix} \begin{bmatrix} \dot{l}_{01} \\ \dot{l}_{02} \\ \dot{\gamma} \end{bmatrix} = [\boldsymbol{G}_{l_1}^{w}]\dot{\boldsymbol{q}} \tag{46}$$

The linear velocity of point B_i ($i = 1,2$) can be obtained as follows

$$\begin{aligned} \boldsymbol{v}_{Bi} &= [\boldsymbol{S}_1 \times B_i \quad \boldsymbol{S}_2 \times B_i \quad 0] \begin{bmatrix} \dot{\alpha} \\ \dot{\beta} \\ \dot{\gamma} \end{bmatrix} \\ &= [\boldsymbol{S}_1 \times B_i \quad \boldsymbol{S}_2 \times B_i \quad 0] \begin{bmatrix} \boldsymbol{J}^{-1} & \boldsymbol{0} \\ \boldsymbol{0} & 0 \end{bmatrix} \begin{bmatrix} \dot{l}_{01} \\ \dot{l}_{02} \\ \dot{\gamma} \end{bmatrix} \end{aligned} \tag{47}$$

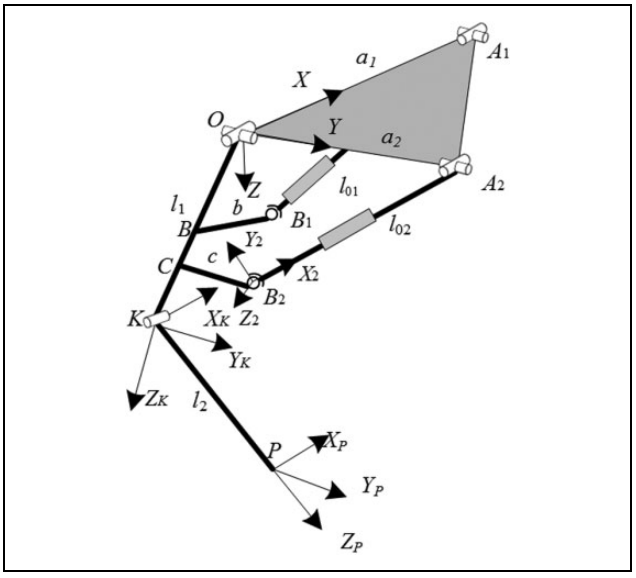


Figure 7. Two branched chain coordination system.

Then setting $[\boldsymbol{S}_1 \times B_i \quad \boldsymbol{S}_2 \times B_i \quad 0]\begin{bmatrix} \boldsymbol{J}^{-1} & \boldsymbol{0} \\ \boldsymbol{0} & 0 \end{bmatrix} = [\boldsymbol{G}_{l_1}^{Bv}]$, equation (47) can be expressed as follows

$$\boldsymbol{v}_{Bi} = [\boldsymbol{G}_{l_1}^{Bv}]\dot{\boldsymbol{q}} \tag{48}$$

where B_i is the distance from the point B_i to the origin O of the fixed coordinate system under the fixed coordinate system O-XYZ.

In the two parallel input UPS branched chain, setting up the coordinate system B_i-$X_iY_iZ_i$ at point B_i, as shown in Figure 7.

According to the motion pairs of the UPS branched chain and based on the influence coefficient method, the linear velocity and angular velocity of point B_i can be expressed as follows

$$\begin{bmatrix} \boldsymbol{w}_{B_i} \\ \boldsymbol{v}_{B_i} \end{bmatrix} = \begin{bmatrix} \boldsymbol{S}_1 & \boldsymbol{S}_2 & \boldsymbol{0} & \boldsymbol{S}_4 & \boldsymbol{S}_5 & \boldsymbol{S}_6 \\ \boldsymbol{S}_1 \times l_{0i} & \boldsymbol{S}_2 \times l_{0i} & l_{0i}/l_{0i} & \boldsymbol{0} & \boldsymbol{0} & 0 \end{bmatrix} \begin{bmatrix} \dot{\varphi}_1 \\ \dot{\varphi}_2 \\ \dot{\varphi}_3 \\ \dot{\varphi}_4 \\ \dot{\varphi}_5 \\ \dot{\varphi}_6 \end{bmatrix} \tag{49}$$

where $\boldsymbol{l}_{0i}$ is the vector coordinate from the Universal pair of the UPS branched chain to the coordinate system origin, and $\dot{\varphi}_i$ is the generalized input velocity of each motion pair of the UPS branched chain.

By solving the inverse matrix of equation (49), and taking out the first two rows of the inverse matrix, the generalized input velocity of each motion pair can be obtained as follows

$$\begin{bmatrix} \dot{\varphi}_1 \\ \dot{\varphi}_2 \end{bmatrix} = [\boldsymbol{G}]\begin{bmatrix} \boldsymbol{w}_{B_i} \\ \boldsymbol{v}_{B_i} \end{bmatrix} = [\boldsymbol{G}]\begin{bmatrix} \boldsymbol{G}_{l_1}^{w} \\ \boldsymbol{G}_{l_1}^{Bv} \end{bmatrix}\dot{\boldsymbol{q}} \tag{50}$$

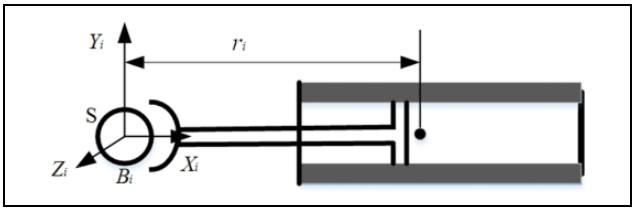


Figure 8. Electric push rod structure.

where $[\boldsymbol{G}]$ is the first two rows which is taken out from the matrix inversion of equation (49).

As shown in Figure 8, suppose the mass of the pushing rod is m_1 and uniform distribution, the length is $2r_1$, and the distance from the initial position to the current position in the electric cylinder is x; the mass of the electric cylinder is m_2 and uniform distribution, the length is $2r_2$. According to the method of calculating the centroid, the centroid of the electric pushing rod is as follows

$$r_i = \frac{m_1 r_1 + m_2(r_2 + x)}{m_1 + m_2} \tag{51}$$

Then, based on the influence coefficient method, the angular velocity and linear velocity of the centroid of the electric pushing rod can be obtained as follows

$$\boldsymbol{w}_{l_{0i}} = [\boldsymbol{S}_1 \quad \boldsymbol{S}_2]\begin{bmatrix} \dot{\varphi}_1 \\ \dot{\varphi}_2 \end{bmatrix} = [\boldsymbol{S}_1 \quad \boldsymbol{S}_2][\boldsymbol{G}]\begin{bmatrix} \boldsymbol{G}_{l_1}^{w} \\ \boldsymbol{G}_{l_1}^{Bv} \end{bmatrix}\dot{\boldsymbol{q}} = [\boldsymbol{G}_{l_{0i}}^{w}]\dot{\boldsymbol{q}} \tag{52}$$

$$\begin{aligned} \boldsymbol{v}_{l_{0i}} &= [\boldsymbol{S}_1 \times r_i \quad \boldsymbol{S}_2 \times r_i]\begin{bmatrix} \dot{\varphi}_1 \\ \dot{\varphi}_2 \end{bmatrix} \\ &= [\boldsymbol{S}_1 \times r_i \quad \boldsymbol{S}_2 \times r_i][\boldsymbol{G}]\begin{bmatrix} \boldsymbol{G}_{l_1}^{w} \\ \boldsymbol{G}_{l_1}^{Bv} \end{bmatrix}\dot{\boldsymbol{q}} = [\boldsymbol{G}_{l_{0i}}^{v}]\dot{\boldsymbol{q}} \end{aligned} \tag{53}$$

The above is the linear speed and angular velocity of the upper leg, lower leg, and the two parallel branch input rods of the robot.

Kinematics simulation

In order to verify the kinematics of the single leg of the robot, the endpoint trajectory of the swing leg and the trotting gait was simulated by the MATLAB software and ADAMS software.[28] After modifying the material properties of the components and adding the constraints, position, and velocity, the robot model was imported into the ADAMS software, as shown in Figure 9.

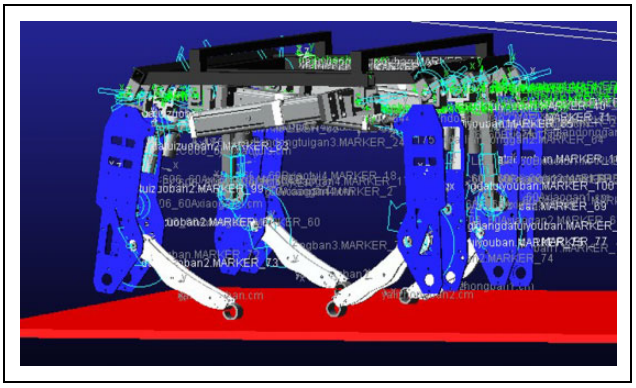


Figure 9. Virtual prototype model of the robot in ADAMS software.

Simulation of the swing leg's endpoint trajectory

The specific simulation process is as follows:

1. A parabola is assumed to be the theoretical trajectory of the lower leg's endpoint, the parabolic equation can be expressed as follows

$$y = -0.04x^2 + 4x \tag{54}$$

2. Based on the kinematics analysis above, the rotation angle α, β, and γ can be obtained by the MATLAB software. Then, the angular velocity and linear velocity of the upper leg and lower leg in one cycle are calculated, the curves are shown in Figure 10. The curves show that both the start velocity and terminal velocity are zero, and the moving velocity is smooth. This verifies that the robot's input joints work smoothly without impact and the established kinematic model is accurate.
3. The position and angular velocities are taken as the input of the model in ADAMS software, then the simulation results are obtained. The comparison of theoretical curve and simulation curve of angular velocity and linear velocity of the lower leg is shown in Figure 11. It can be seen that the simulation curve coincides with the theoretical curve basically. There is no difference of angular velocity and linear velocity, and the soft landing can be achieved.

In order to select the individual drives for the robot's leg mechanism, the required forces and torques of the drives need to be known. In Figure 12, the driving force of the electric push rod and the torque of the motor in the process of the leg steps forward were simulated. It can be seen from the figure, the curves are stable and smooth, without mutation, so the electric push rod and the motor will not have huge shock and vibration. The driving force of the electric push rod and the torque of the motor were known, and these

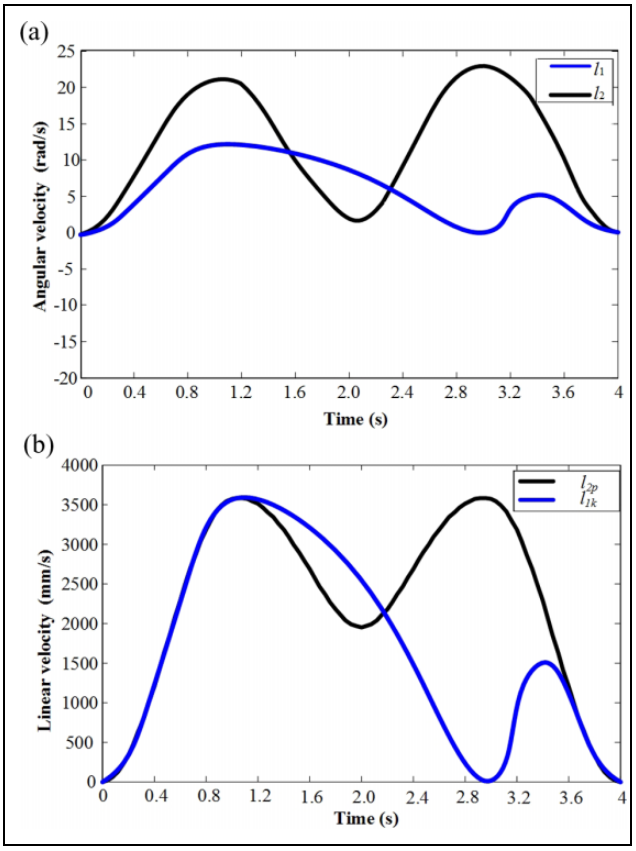


Figure 10. Curves of angular velocity and linear velocity of the upper leg and lower leg in one cycle. (a) Curves of the angular velocity of the upper leg and lower leg. (b) Curves of linear velocity of the endpoint of the upper leg and lower leg.

will provide a theoretical basis for selecting the individual drives.

Simulation of the trotting gait

The dynamic simulation of the robot's trotting gait is shown in Figure 13. The velocity curve of the robot body is shown in Figure 14, it can be seen that the robot body moves smoothly and has no impact, and the speed of the robot body can be very fast, and the curve conforms to the established model. In Figure 15, it can be seen that the robot's center of gravity changes very small, about 0.9 mm. This shows that the center of gravity of the robot is stable in the trotting gait. This avoids frequent changes in the height of the center of gravity, causing the robot to collapse easily.

Experimental research on the single leg mechanism of the robot

The experiment of single leg mechanism is the basis of experiment of the whole robot, so only one single leg prototype was made at first. The single leg of the robot has two electric pushing rods and one motor; thus, the single leg

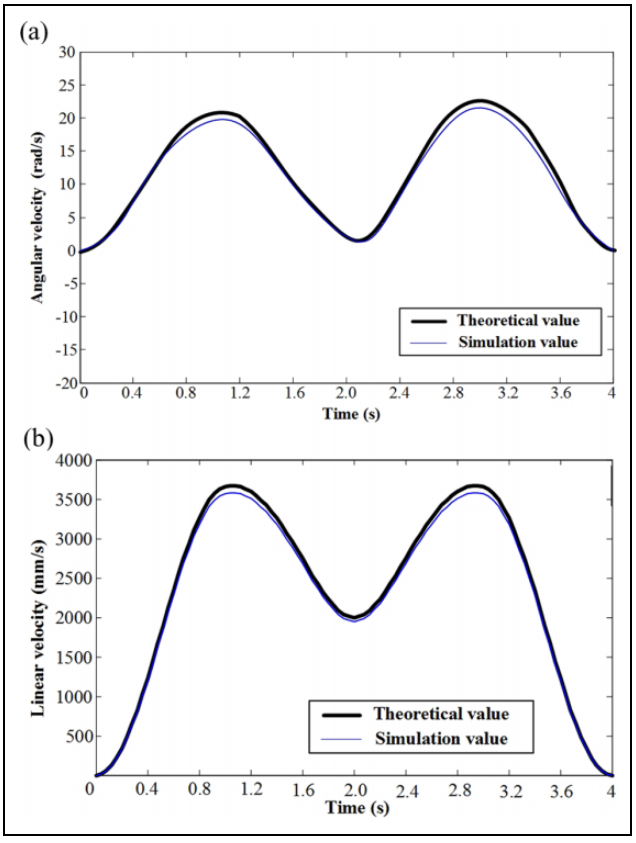


Figure 11. (a) Comparison of theoretical curve and simulation curve of angular velocity of the lower leg. (b) Comparison of theoretical curve and simulation curve of linear velocity of the lower leg's endpoint.

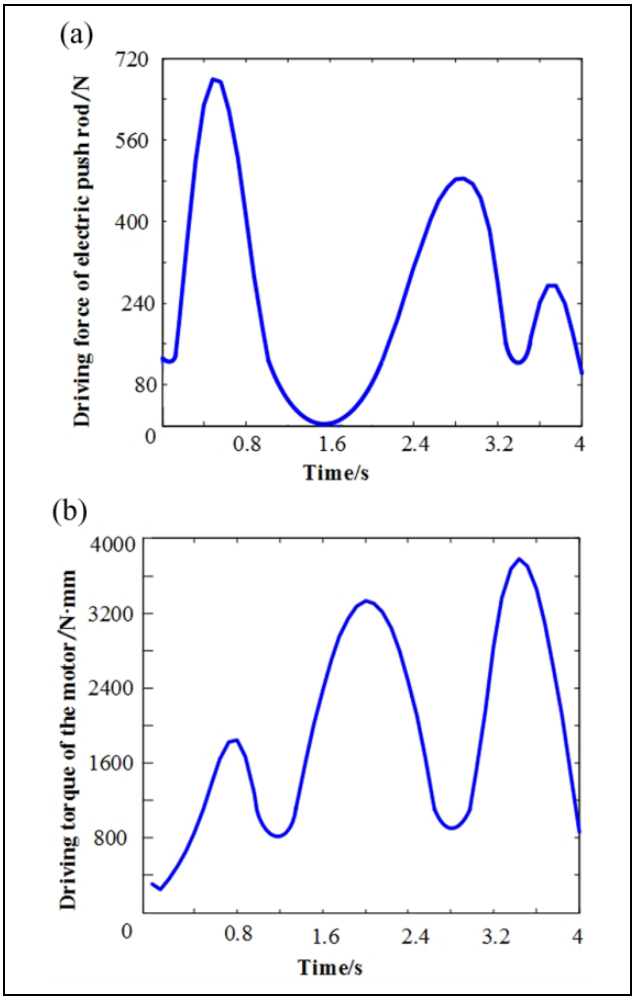


Figure 12. Required driving force and torque of the input joint. (a) Driving force of electric push rod and (b) driving torque of the motor.

prototype system includes the single leg mechanism, three controller, three drives, two power-supply module, and one PC, as shown in Figure 16.

Motion experiment of the single leg mechanism

Based on the above components, building the robot control system and according to the kinematics analysis of the single leg mechanism, the motion of the single leg mechanism of the robot is obtained, as shown in Figure 17. It can be seen that the single leg prototype moves continuously and stable without large fluctuation, and the input joints are within their range of motion.

Trajectory tracking experiment of the single leg mechanism

The motion experiment above shows the feasibility of the motion of the single leg but cannot explain whether the trajectory of the endpoint of the single leg is consistent with the theoretical trajectory. Therefore, the trajectory tracking measurement experiment of the endpoint of the single leg was completed with the laser tracker,[29] as shown in Figure 18.

The process of the whole experiment is as follows:

1. The initial position of the endpoint of the single leg is measured by using the Leica T-Probe handheld measuring sensor, and the raw data are saved.
2. The reflection ball is fixed on the endpoint of the single leg and it reflects the laser.
3. The reference point of the endpoint of the single leg mechanism moves according to the planning trajectory, then repeat the experiment five times, and the data are collected and stored in the track output interface, as shown in Figure 19. The comparison of theoretical trajectory curve and actual trajectory curve of the lower leg's endpoint is obtained by the MATLAB software, as shown in Figure 20. It can be seen that the actual trajectory of the lower leg's endpoint coincides with the theoretical trajectory basically, but there are errors also. The errors are mainly due to the machining error and assembly error of the mechanism.

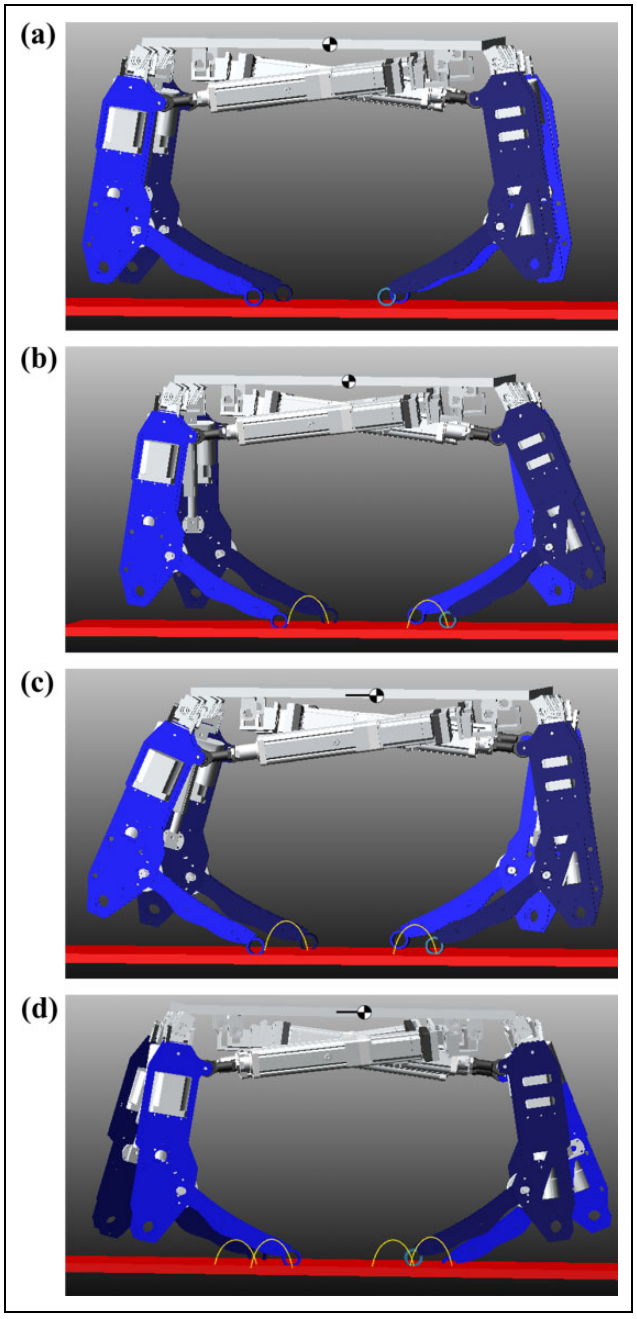


Figure 13. Dynamic simulation of the robot's trotting gait. (a) Initial time, (b) legs 1 and 3 move forward, (c) forward movement of the robot body, and (d) legs 2 and 4 move forward.

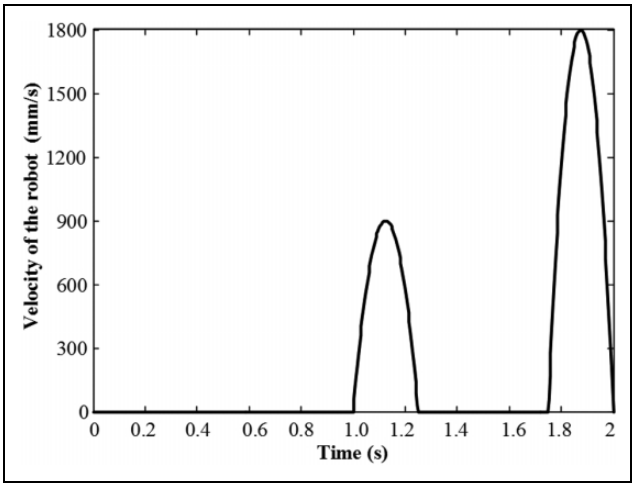


Figure 14. Velocity curve of the robot body.

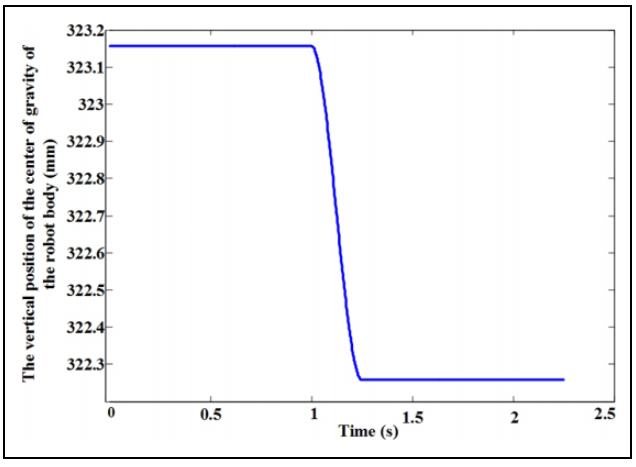


Figure 15. Changes in the vertical position of the center of gravity of the robot body.

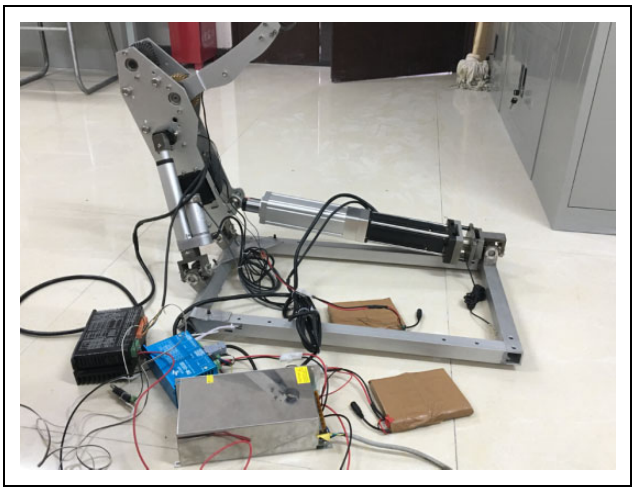


Figure 16. Single leg prototype system of the robot.

Conclusion

1. This article proposes a novel rescue robot with the (2-UPS+U) &R serial–parallel and wheel-legged mechanism. The DOFs of the single leg mechanism and the whole machine were calculated. The forward and backward position solutions of the swing leg and the standing leg were analyzed and the work space of the leg mechanism was carried out. The above research verified that the leg mechanism can meet the requirement of walking in the unstructured environment. And it will provide the basis for the following trajectory planning and gait planning.

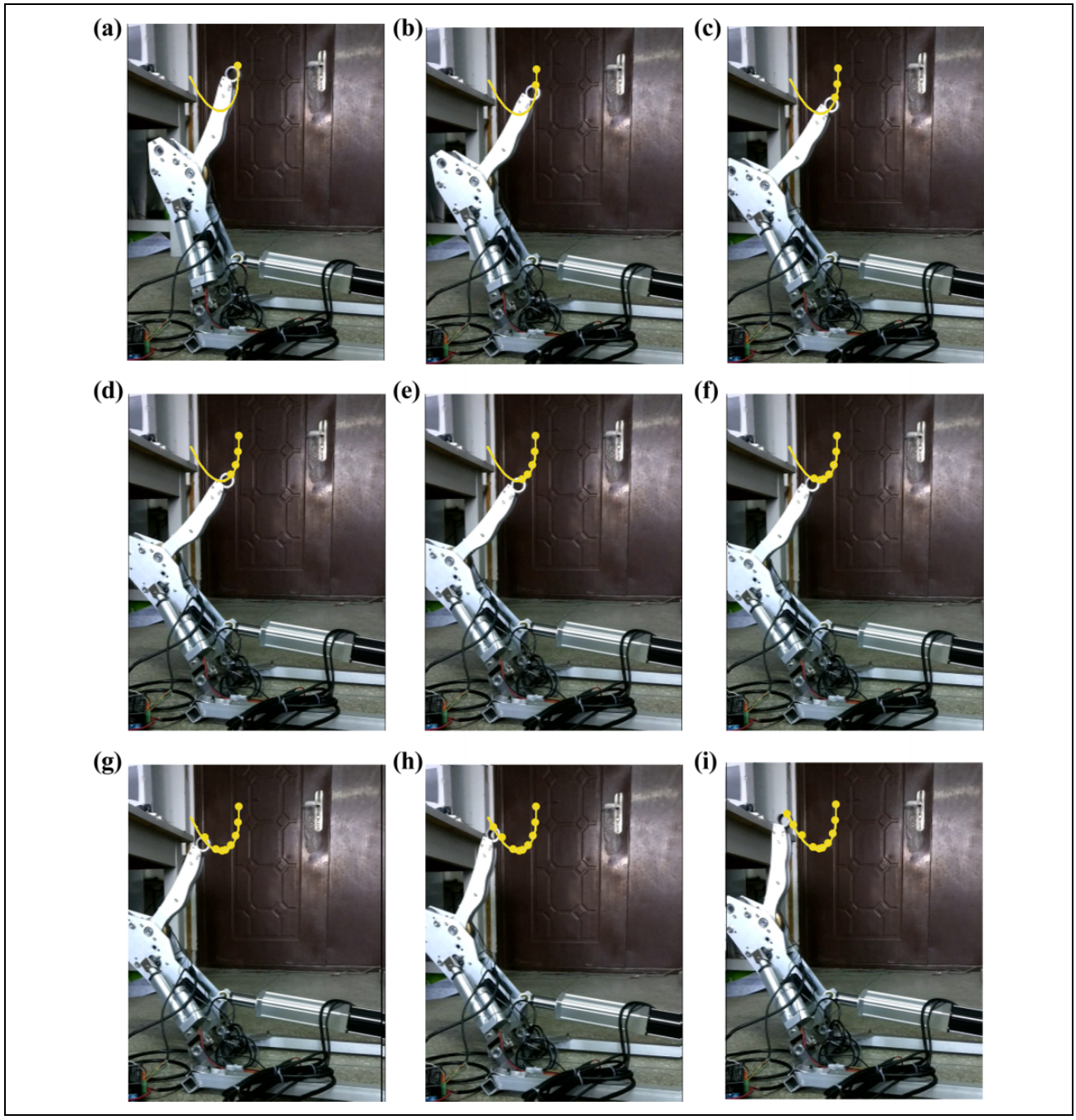


Figure 17. Motion of the single leg mechanism of the robot. (a) Initial position, (b) to (d) process of stepping forward, (e) reach the highest point, (f) to (h) process of withdrawing the leg back, and (i) return to the initial position.

2. The Jacobi matrix between the input joints and output joints of the swing leg was established. According to the influence coefficient method, the linear velocity and angular velocity of each rod's centroid of the leg mechanism were solved, and the velocity was expressed as a function of the generalized input angle. So, the foundation for dynamics analysis was obtained.
3. Then, the 3-D model of the robot is imported into the ADMAS software, and based on the above research, the simulation is finished with the MATLAB software. The kinematic analysis of the leg mechanism is verified.
4. Based on the prototype of the single leg mechanism, the motion experiment of the single leg mechanism was realized. The trajectory tracking experiment was carried out, and the actual trajectory of the lower leg's endpoint coincides with the theoretical trajectory basically, which verifies the feasibility of the novel leg mechanism.

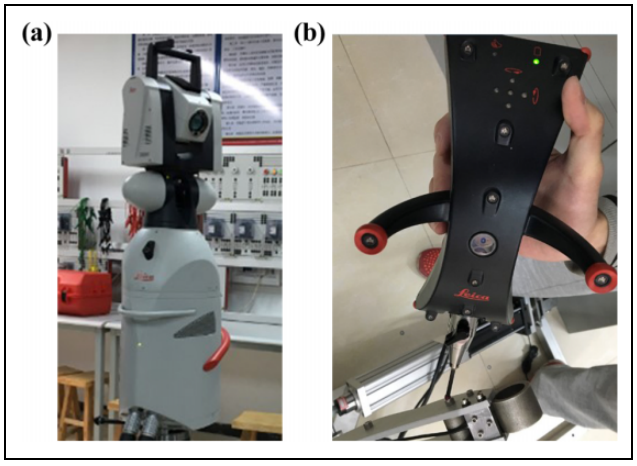


Figure 18. Experiment of trajectory tracking measurement. (a) Laser tracker and (b) establishing the coordinate system and measuring the initial position.

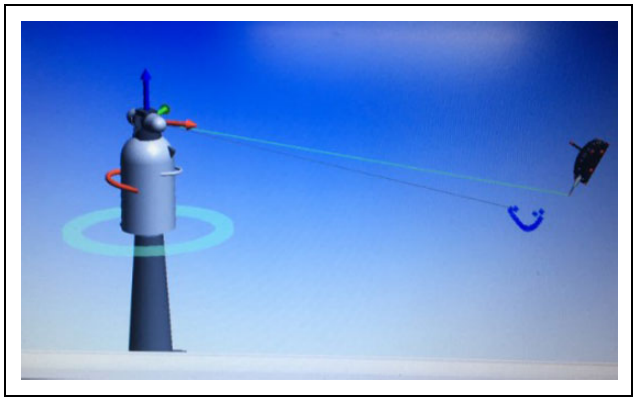


Figure 19. Track output interface.

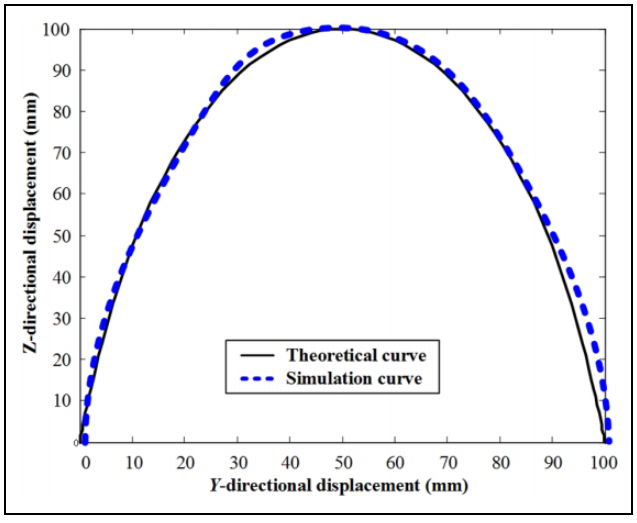


Figure 20. Comparison of theoretical trajectories and actual trajectories.

In the future, the dynamics analysis of the robot will be solved by the Lagrange equation, which will solve the relationship between the driving force and the required speed, and the base will be established for the robot control. The stability criterion and gait planning of the robot will be researched. The robot prototype will be finished and the above problems will be verified.

Declaration of conflicting interests

The author(s) declared no potential conflicts of interest with respect to the research, authorship, and/or publication of this article.

Funding

The author(s) disclosed receipt of the following financial support for the research, authorship, and/or publication of this article: This work was partially supported by the EU H2020 Project-SMOOTH (project no. 734875), the EU FP7-PEOPLE-2012-IRSES Project-RABOT (project no. 318902), and the Collaborative Innovation Project of College of Mechanical Engineering, Yanshan University, Hebei Province (project no. JX2014-01).

References

1. Duchoň F, Hubinský P, Hanzel J, et al. Intelligent vehicles as the robotic applications. *Procedia Eng* 2012; 48: 105–114.
2. Alnounou Y, Haidar M, Paulik M, et al. Service-oriented architecture: on the suitability for mobile robots. In: *2010 IEEE international conference on electro/information technology*, Normal, IL, USA, 20–22 May 2010, p. 1–5. IEEE Computer Society.
3. Cesetti A, Scotti CP, Di Buò G, et al. A service oriented architecture supporting an autonomous mobile robot for industrial applications. In: *18th Mediterranean conference on control and automation*, Marrakech, Morocco, 23–25 June 2010, pp. 604–609. IEEE Computer Society.
4. Cai Z. *Robotics*. 2nd ed. Beijing: Tsinghua University Press, 2009, pp. 14–17 (in Chinese).
5. Eisen HJ, Wen LC, Hickey G, et al. Sojourner Mars rover thermal performance. In: *28th international conference on environmental systems*, Danvers, MA, USA, 13–16 July 1998, pp. 13–13. SAE International.
6. Wilcox BH, Litwin T, Biesiadecki J, et al. Athlete: a cargo handling and manipulation robot for the moon. *J Field Robot* 2007; 24(5): 421–434.
7. Endo G and Hirose S. Study on roller-walker (multi-mode steering control and self-contained locomotion). In: *IEEE international conference on robotics and automation*, Vol. 3, San Francisco, CA, USA, 24–28 April 2000, pp. 2808–2814. IEEE.
8. Endo G and Hirose S. Study on roller-walker improvement of locomotive efficiency of quadruped robots by passive wheels. *Adv Robot* 2012; 26(8–9): 969–988.
9. Hiller M.Virtual prototyping of the combined wheeled and legged robot ALDURO. *Romansy 14-Theory and Practice*

of Robots and Manipulators, Vol. 438, Vienna: Springer, 2002, p. 3.
10. Grand C, BenAmar F, Plumet F, et al. Stability and traction optimization of a reconfigurable wheel-legged robot. *Int J Robot Res* 2004; 23(10–11): 1041–1058.
11. Lauria M, Piguet Y, and Siegwart R. Octopus: an autonomous wheeled climbing robot. In: *5th international conference on climbing and walking robots*, Paris, France, 25–27 September 2002, pp. 315–322.
12. Gronowicz A, Sperzyński P, Szrek J, et al. Wheel-legged robot: construction and obstacle detection sensors. *Mech Mach Sci* 2014; 17: 191–198.
13. Smith JA, Sharf I and Trentini M. PAW: a hybrid wheeled-leg robot. In: *IEEE international conference on robotics and automation*, Orlando, FL, USA, 15–19 May 2006, pp. 4043–4048. IEEE.
14. Huang B, Wang P, and Sun L. Behavior-based control of a hybrid quadruped robot. In: *World congress on intelligent control & automation*, Vol. 2, Dalian, China, 21–23 June 2006, pp. 8997–9001. IEEE.
15. Pengfei W and Lining S. Wheeled foot quadruped robot HITAN-I. *High Technol Lett* 2006; 12(4): 346–350.
16. Yang F, Ding X, and Peng S. Bio-control of a modular design robot-NOROS. In: *Third ASME/IFToMM International Conference on Reconfigurable Mechanisms and Robots (ReMAR 2015)*, Beijing, China, 20–22 July 2015, pp. 891–900. London: Springer.
17. Lu D, Dong E, Liu C, et al. Design and development of a leg-wheel hybrid robot "HyTRo-I." In: *IEEE/RSJ international conference on intelligent robots and systems (IROS)*, Tokyo, Japan, 3–7 November 2013, pp. 6031–6036. IEEE.
18. Chen SC, Huang KJ, Chen WH, et al. Quattroped: a leg-wheel transformable robot. *IEEE/ASME Trans Mech* 2014; 19(2): 730–742.
19. Luo Y, Li Q, and Liu Z. Design and optimization of wheel-legged robot: rolling-wolf. *Chin J Mech Eng (English Ed)* 2014; 27(6): 1133–1142.
20. Hirose S. Three basic types of locomotion in mobile robots. In: *Fifth international conference on advanced robotics-91 ICAR*, Pisa, Italy, 19–22 June 1991, pp. 12–17. IEEE.
21. Hu B. *Theoretical study of limited-DOF parallel manipulators and serial-parallel manipulators based on constrained force/torque*. PhD Thesis, Yanshan University, Qinhuangdao, China, 2010, pp. 1–15 (in Chinese).
22. Sang L, Wang H, and Sun L. Analysis of DOFs of human-carrying waking chair robot and arrangements of moving platform of leg mechanism. *J Yanshan Univ* 2013; 37(4): 317–325 (in Chinese).
23. Zhang M and Zhuo B. Workspace analysis and parameter optimization of a six DOF 6-3-3 parallel link machine tool. In: *2nd international conference on intelligent robotics and applications, ICIRA*, Singapore, 16–18 December 2009, pp. 706–712. Springer Verlag.
24. Wang H, Sang L, Hu X, et al. Kinematics and dynamics analysis of a quadruped walking robot with parallel leg mechanism. *Chin J Mech Eng* 2013; 26(5): 881–891.
25. Yang P and Gao F. Leg kinematic analysis and prototype experiments of walking-operating multifunctional hexapod robot. *Proc Instit Mech Eng C J Mech Eng Sci* 2014; 228(12): 2217–2232.
26. Huang Z, Zhao YS and Zhao TS. *Advanced spatial mechanism*. Beijing: Higher Education Press, 2006, pp. 65–212 (in Chinese).
27. Huang T, Wang JS, Gosselin CM, et al. Kinematic synthesis of hexapods with specified orientation capability and well-conditioned dexterity. *J Manuf Proc* 2000; 2(1): 36–47.
28. Yuan Z, Zhu W, Wang D, et al. Kinematics analysis and simulation of a 7-DOF welding robot based on ADAMS and MATLAB. In: *Advances in computer, communication, control and automation*, vol. 121, Zhuhai, China, 19–20 November 2011, pp. 633–640. Springer Verlag.
29. Sang L, Wang H, Yu H, et al. A novel human-carrying quadruped walking robot. *Int J Adv Robot Syst* 2017; 7: 1–17.